Phys. Status Solidi B **251,** No. 11, 2159–2168 (2014) / **DOI** 10.1002/pssb.201400022

physica status solidi b
www.pss-b.com
basic solid state physics

Feature Article

Stress and doping impact on intrinsic point defect behavior in growing single crystal silicon

Koji Sueoka[*,1], Eiji Kamiyama[,1], Jan Vanhellemont[***,2], and Kozo Nakamura[****,1]**

[1] Department of Communication Engineering, Okayama Prefectural University, 111 Kuboki, Soja, Okayama 719-1197, Japan
[2] Department of Solid State Sciences, Ghent University, Krijgslaan 281-S1, 9000 Gent, Belgium

Received 1 April 2014, accepted 3 June 2014
Published online 26 September 2014

Keywords density functional theory, dopant, intrinsic point defect, single crystal silicon, thermal stress

[*] Corresponding author: e-mail sueoka@c.oka-pu.ac.jp, Phone: +81 866 94 2136, Fax: +81 866 94 2199
[**] e-mail ejkamiyama@aol.com, Phone: +81 866 94 2136, Fax: +81 866 94 2199
[***] e-mail jan.vanhellemont@ugent.be, Phone: +32 499593857, Fax: +32 92644996
[****] e-mail kozo_nakamura@nifty.ne.jp, Phone: +81 866 94 2136, Fax: +81 866 94 2199

For the mass-production of 450 mm-diameter defect-free Si crystals, one has to take into account the impact of thermal stress on intrinsic point defect properties and behavior during single crystal growth from a melt. Very recently, first experimental evidence was published that the compressive thermal stress near the melt/solid interface makes a growing 300 mm diameter Czochralski Si crystal more vacancy-rich. In order to explain these experimental results quantitatively, the dependence of the formation enthalpies of the vacancy (V) and the self-interstitial (I) on compressive plane stress was determined using density functional theory (DFT) based calculations. It is found that compressive plane stress gives a higher stress dependence of the so-called "Voronkov criterion" compared to isotropic stress. The calculated plane stress dependence is in excellent agreement with the published experimental values and should be taken into account in the development of pulling processes for 450 mm diameter defect-free Si crystals. Also, the mechanisms behind the experimentally observed impact of the type and concentration of substitutional dopants on intrinsic point defect behavior and formation of grown-in defects are clarified. On the basis of the DFT calculated results, an appropriate model of intrinsic point defect behavior in heavily doped Si is proposed. (i) The incorporated total V and I concentrations at the melting point depend on the types and concentrations of dopants. (ii) Most of the total V and I concentrations contribute to Frenkel pair recombination during Si crystal growth at temperatures much higher than those to form grown-in intrinsic point defect clusters. The Voronkov model, while taking into account the present improvements, clearly explains all reported experimental results on grown-in defects for heavily doped Si. The most important remaining problems with respect to intrinsic point defect behavior and properties during single crystal growth from a melt are also discussed.

1 Introduction Nowadays, defect-free Si wafers containing no measurable grown-in intrinsic point defect clusters are standard in 300 mm-diameter wafer production. As discussed in this paper, for the development and mass-production of 450 mm-diameter defect-free Si crystals, one will have to take into account the impact of thermal stress on intrinsic point defect properties and behavior during single crystal growth from a melt. The control of the delicate balance of vacancies (V) and self-interstitials (I) during crystal pulling is based on the so-called "Voronkov criterion" [1]. According to this criterion, a crystal that is pulled with the ratio (v/G) of the pulling speed v over the axial temperature gradient G at the melt/solid interface, larger than a critical value $(v/G)_{crit}$, is vacancy-rich while when (v/G) is smaller than the critical value, the pulled crystal is self-interstitial-rich. The "Voronkov criterion" $(v/G)_{crit}$ can be written as [2]

$$\left(\frac{v}{G}\right)_{crit} = \frac{C_I^{eq}(T_m)D_I(T_m)(E+Q_I) - C_V^{eq}(T_m)D_V(T_m)(E+Q_V)}{k(T_m)^2(C_V(T_m)-C_I(T_m))}$$
$$\text{with } E = \frac{E_f^I + E_f^V}{2}, \quad (1)$$

where C_I, C_I^{eq}, and C_V, C_V^{eq} are the actual and the thermal equilibrium I and V concentrations, respectively. D_I and D_V are the I and V diffusivities, respectively. Q_I and Q_V are the

reduced heats of transport of I and V, respectively, defined as the heat flux per unit flux of component atom in the absence of temperature gradient. T_m is the melt temperature and k is the Boltzmann constant. E_f^I and E_f^V are the formation energy of I and V, respectively. By evaluating the Voronkov criterion, Nakamura et al. [3] very recently published for the first time clear experimental evidence that the compressive thermal stress near the melt/solid interface shifts the growing Czochralski Si crystal to more vacancy-rich.

The Voronkov criterion is also affected by the type and concentration of dopants. For example, the reduction of the radius of the oxidation induced stacking fault (OSF) ring in CZ-Si in case of B doping higher than $\sim 1 \times 10^{18}$ B cm^{-3} indicates that $(v/G)_{crit}$ is increased by heavy B doping [4]. On the contrary, P, As, and Sb make the crystal more V-rich [5]. However, the mechanism behind the experimentally observed impact by dopants has not been clarified so far.

The purpose of this paper is to review our recent studies of the dependence of Voronkov criterion on the thermal stress [6–10] and the dopant [11] by using density functional theory (DFT) based calculations. An illustration of a result that is useful for practical application, is the predicted process window for future defect-free large-diameter Si crystals. An appropriate model of intrinsic point defect behavior in growing heavily doped Si is also proposed. When taking into account the results of the present study, the Voronkov model successfully explains the reported experimental results of the impact of thermal stress and dopant on the intrinsic point defect behavior. Finally, the most important remaining problems related to the topic of the present paper will be discussed.

2 Impact of stress on the Voronkov criterion [8–10]

2.1 Results of DFT study for isotropic stress A detailed DFT study has been performed to evaluate the pressure dependence of both the formation enthalpy (H_f) and the migration enthalpy (H_m) of the intrinsic point defects [8, 9]. It was found that the pressure-induced change of H_m is much smaller than that of H_f. By assuming that the thermal stress is internal and isotropic in the bulk of the crystal (hereinafter referred to as "isotropic"), the *ab initio* calculations predicted that compressive thermal stress shifts the growing Si crystal towards more vacancy-rich.

The dominant component of the thermal stress near the melt/solid interface in most of the central region of the growing crystal is, however, internal and compressive plane stress [12]. If the local strain around a point defect is assumed to isotropic, the impact of stress depends on the value of mean stress independent of the stress type. However, the local strain around a point defect in the ground state, for example a vacancy of D_{2d} symmetry with Jahn–Teller distortion [13], is anisotropic. In order to evaluate the impact of thermal stress on the critical $(v/G)_{crit}$ more accurately, it is therefore essential to evaluate the dependence of the formation enthalpies of V and I on compressive plane stress near the melt/solid interface [10].

2.2 Calculation details for plane stress Details on the DFT calculation procedure used for bulk-isotropic stress can be found in Refs. [8, 9]. For the case of plane stress, we assumed internal and (110) planar-isotropic (hereinafter referred to as "plane") stress [10]. The reference points were the perfect Si crystals deformed with changing cell sizes of $L_x = L_y = L$ and keeping L_z free. The ionic coordinates were fully relaxed to build up a list of (total energy: E_{tot}) – (mean plane stress: $\sigma_{ave} = (\sigma_x + \sigma_y)/3$) – (cell size and volume: L_x, L_y, L_z and Vol $= L_x L_y L_z$) data points. Similar calculations were performed for rectangular supercells containing point defects with changing cell sizes of $L_x = L_y = L$ and keeping L_z free.

In the present study, only neutral intrinsic point defects with lowest energy configurations, i.e., the vacancy with D_{2d} symmetry and Jahn–Teller distortion in Fig. 1a, and the self-interstitial [110] dumbbell (D), were considered. In case of (110) plane stress, both the [110] D-site (with the Si dumbbell contained in the (110) plane) and the [10$\bar{1}$] D-site (with the Si dumbbell not contained in the (110) plane) in Fig. 1b were calculated.

The data points described above were used to obtain the relationship between the average stress σ_{ave}, (i) the formation energy E_f and (ii) the relaxation volume $\Delta V_x + \Delta V_y$ in the (110) plane. Here, $\Delta V_x + \Delta V_y$ is the volume change in the (110) plane with respect to the perfect crystal due to V or I formation. The formation enthalpies of V and I for $\sigma_{ave} = (\sigma_x + \sigma_y)/3$ can be written as

$$H_f^{V,I}(\sigma_{ave}) = E_f^{V,I}(\sigma_{ave}) + (\sigma_x \cdot \Delta V_x^{V,I}(\sigma_x) + \sigma_y \cdot \Delta V_y^{V,I}(\sigma_y)). \quad (2)$$

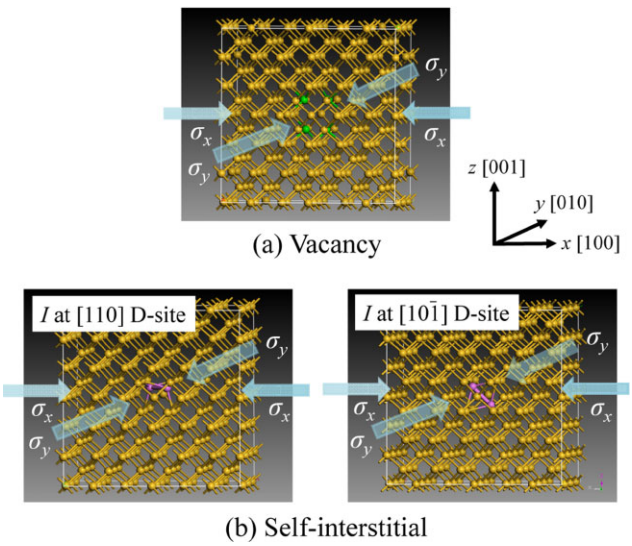

Figure 1 Geometries of (a) vacancy of D_{2d} symmetry with Jahn–Teller distortion, and (b) [110] and [10$\bar{1}$] dumbbell (D) self-interstitials, in a 216 atoms supercell. The four green atoms in (a) form a vacancy while the two pink atoms in (b) form a D-site self-interstitial.

2.3 Calculated results of formation enthalpy

Figure 2a and b shows the change of formation enthalpies H_f^V and H_f^I due to plane or isotropic stress. It was found that H_f^V decreases while H_f^I increases with increasing compressive stresses. Furthermore, the $[10\bar{1}]$ D-site is more stable compared to [110] D-site in case of compressive plane stress.

The calculations lead to dependencies of H_f^V and H_f^I on σ_{ave} ($-1\,\text{GPa} < \sigma_{ave} < 0\,\text{GPa}$) given by

$$H_f^V(\text{eV}) = \begin{cases} 0.308 \cdot \sigma_{ave}\,(\text{plane}) \\ 0.153 \cdot \sigma_{ave}\,(\text{isotropic}) \end{cases} \quad (3a)$$

and

$$H_f^I(\text{eV}) = \begin{cases} -0.069 \cdot \sigma_{ave}\,(\text{plane}) \\ -0.068 \cdot \sigma_{ave}\,(\text{isotropic}) \end{cases} \quad (3b)$$

with σ_{ave} given in GPa. For V, the impact of plane stress is thus about two times larger than for isotropic stress. This is due to the larger flexibility of Si atoms around the Jahn–Teller distorted V under plane stress. On the other hand, for I, the impact of plane stress is almost the same as for isotropic stress.

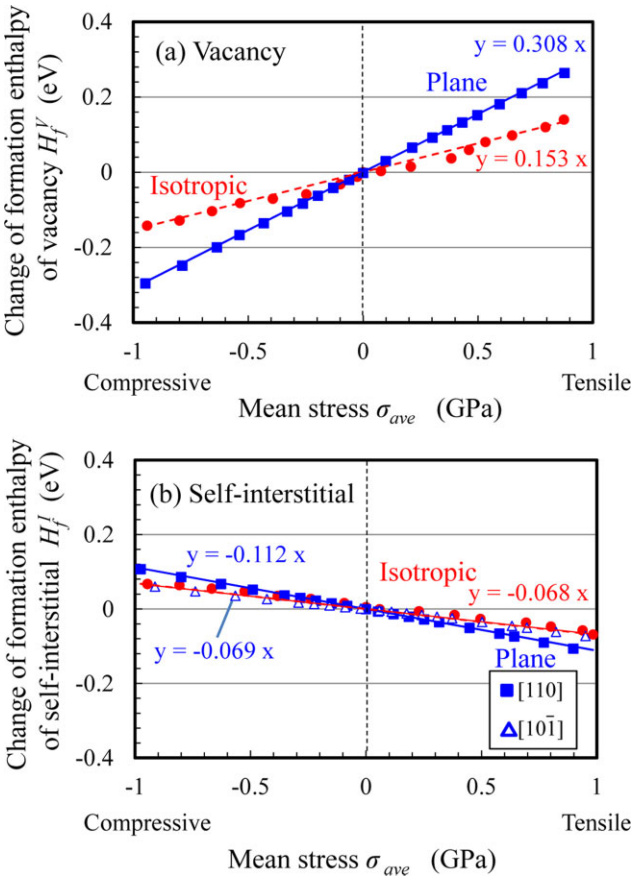

Figure 2 Calculated dependencies of formation energies (a) E_f^V and (b) E_f^I, on mean plane or isotropic stresses σ_{ave} between -1 GPa (compressive) and 1 GPa (tensile).

2.4 Dependence of the Voronkov criterion on plane and isotropic stresses

The impact of compressive thermal stress on $(v/G)_{crit}$ is estimated by replacing the formation energies in Eq. (1) by the enthalpies obtained in this study and by using the thermal equilibrium concentrations at melt temperature, corresponding with these new formation enthalpies assuming at this moment that the pre-exponential factors are not affected. To illustrate the impact of compressive thermal stress, the values of the formation enthalpies as a function of mean thermal stress σ_{ave}^{th} given by Eqs. (3a) and (3b) were used. For the analysis at $\sigma_{ave}^{th} = 0$, the thermal equilibrium concentrations and the diffusivities of point defects extracted from single crystal Si growth experiments by Nakamura et al. [14] were used as their parameters reproduced well the two dimensional defect distribution they observed in Czochralski-grown Si crystals.

Figure 3 shows the comparison of the theoretical and experimental $(v/G)_{crit}$ dependence on σ_{ave}^{th} up to -20 MPa. Since the different hot zone between crystals A, B and crystals C, D gave slight differences in the $(v/G)_{crit}$ values for the same calculated σ_{ave}^{th}, the comparisons were performed for crystals A, B (upper figure) and crystals C, D (lower figure), separately [12]. For crystals C and D, we used the more reliable data point sets obtained during decreasing growth rate [12]. Furthermore, it should be noted that the experimental $(v/G)_{crit}$ values for stress levels between 0 and -5 MPa were obtained near the periphery of the wafers so that lateral out-diffusion of the intrinsic point defects and the shape of the melt/solid interface will have an important influence on the extracted $(v/G)_{crit}$ value [3]. As these influences are not taken into account in the simple Voronkov criterion, the data points between 0 and -5 MPa are not included in the comparison. Therefore, the experimental stress dependencies of $(v/G)_{crit}$ values were obtained from the data in the crystal central region for stresses between -5 and -20 MPa shown as dotted line in each figure. The theoretical values (blue full and red dashed lines) were fitted to the value of the dotted line at $\sigma_{ave}^{th} = 0$. The plane stress dependence of $(v/G)_{crit}$ agrees better with the experimental values than the isotropic stress dependence.

In these figures, the windows for defect-free Si are also shown by colored bands [9, 15, 16]. These figures are useful for the development of future large-diameter defect-free Si crystals. It should be stressed that the required process control level is very severe as the window for defect-free Si is quite narrow and is only about $\pm 0.005\,\text{mm}^2\,\text{K}^{-1}\,\text{min}^{-1}$ even for constant σ_{ave}^{th}, which is equivalent to a few MPa under constant v/G. The *ab initio* calculated results for compressive plane stress obtained in the present work will contribute to a more accurate prediction of $(v/G)_{crit}$ for the mass-production of 450 mm diameter defect-free Si crystals.

3 Impact of doping on the Voronkov criterion [11]

3.1 Review of experimental observations

The impact of doping on intrinsic point defect clusters formed during single crystal Si growth from a melt has already been recognized at the early beginning of commercial single

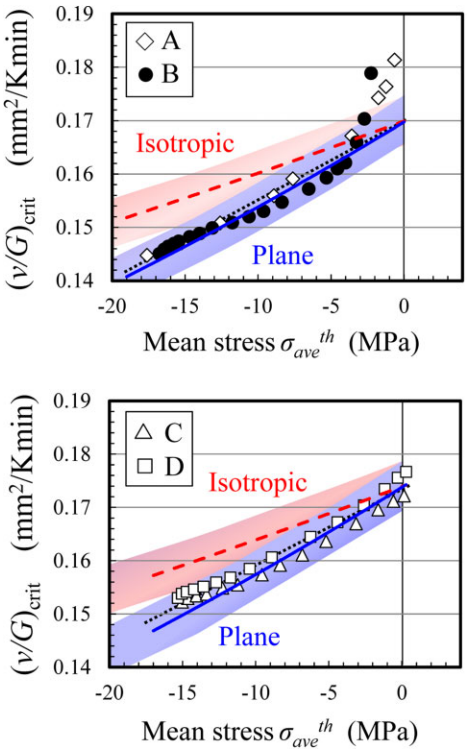

Figure 3 Calculated (blue full and red dashed lines) and experimental $(v/G)_{crit}$ data (symbols) as a function of compressive mean thermal stress σ_{ave}^{th} up to −20 MPa. "A" and "B" in upper figure and "C" and "D" in lower figure are taken from Ref. [3]. The dotted lines are the best fits to the experimental results between −5 and −20 MPa. The theoretical values were fitted to the value of the dotted line at $\sigma_{ave}^{th} = 0$. The windows for defect-free Si pulling are shown by colored bands.

crystal growth process development. Transmission electron microscopy investigations have revealed, e.g., small self-interstitial (I) dislocation clusters in 3×10^{18} B cm^{-3} doped Czochralski-grown Si samples while only vacancy (V) inclusions have been observed in case of 1.2×10^{18} Sb cm^{-3} doping [17]. Abe et al. [18] also studied the effect of N, C, and O doping of floating-zone-grown Si crystals in addition to the effect of electrically active dopants, revealing that V-type point defect clusters were strongly suppressed for N and C doping while O doping led to an increased formation of V clusters.

Dornberger et al. [4] more recently found that the radius of the oxidation induced stacking fault (OSF) ring is reduced in CZ-Si in case of B doping higher than $\sim 1 \times 10^{18}$ B cm^{-3}. Furthermore, Si crystals were found to become I-rich with the OSF ring disappearing in the crystal center for B concentrations higher than $\sim 1 \times 10^{19}$ B cm^{-3}. Nakamura et al. [5] published results of an extensive study on the effects of seven impurities, i.e., B, C, O, N, Sb, P, and As on grown-in defects in CZ-Si crystals. They concluded that doping with high concentrations of these impurities leads to significant changes in the equilibrium concentrations of intrinsic point defects. B and C doping made the crystal more I-rich while O, P, As, and Sb doping made the crystal more V-rich. N doping strongly suppressed V-type point defect clusters despite the increased total concentration of V. Abe [19] recently investigated heavily doped FZ-Si and found that Sn and Sb doping leads to more V-rich crystals while B and C doping leads to more I-rich crystals. Vanhellemont et al. [20] reported that Ge doping at 1×10^{20} Ge cm^{-3} of CZ-Si has only a limited impact on V concentration.

Several mechanisms to explain the observed impact of dopants have already been identified, i.e., (i) local strain (stress) related to dopant atom size [21, 22], (ii) lattice strain (stress) related to dopant atom size [19], (iii) change of the Fermi level [5, 23], and (iv) change of the V and I formation energies around dopant atoms (incorporation of V and I with dopant atoms from melt) [5, 23]. We verified these models in a previous study to explain the experimental results and concluded that the former three mechanisms (and their combinations) did not successfully explain the impact of n-type doping [23]. For those reasons also the last mechanism (iv) should be taken into account. However, no quantitative theoretical analyses have been conducted so far as there are many lattice sites to be considered, especially for self-interstitials around dopant atoms.

3.2 Calculation details for point defects around dopant atoms

In the present paper, an appropriate model of intrinsic point defect behavior in growing heavily doped Si is proposed on the basis of DFT calculations to obtain the formation energies of V and I at all sites within a sphere with 6 Å radius around the dopant atom for V and with 5 Å radius for I. Substitutional p-type (B and Ga), neutral (C, Ge, and Sn) and n-type (P, As, Sb, and Bi) dopants were considered.

Only neutral intrinsic point defects were considered. The formation energy of V or I within a sphere with 6 Å radius or 5 Å radius around the dopant atom is calculated as follows. The cell size of a perfect 216-atom supercell after its geometry is optimized, is 16.392 Å.

A dopant atom is introduced at the center of perfect 216-atom supercells and a vacancy is placed at the 1st to 5th neighbors from the dopant atom (within a sphere with 6 Å radius around the dopant atom). Figure 4 shows the sites of V from the dopant atom at the #0 site by using a quarter of 64-atom supercell ($2a \times a \times a$). The formation energy of V at each site is calculated by fully relaxing the ionic coordinates. The number of site at 1st to 5th neighbors from the dopant at #0 is 4 (1st), 12 (2nd), 12 (3rd), 6 (4th), and 12 (5th), respectively.

Next, a self-interstitial I is placed at known interstitial sites around the dopant atom at #0 in a diamond structure (within a sphere with 5 Å radius around the dopant atom). The geometries of I at the tetrahedral (T), the hexagonal (H), the [110] dumbbell (D), the [100] D, and [114] D-site are considered. The formation energy of I for each site is calculated by fully relaxing the ionic coordinates. Further details on calculation procedures are given in Ref. [11].

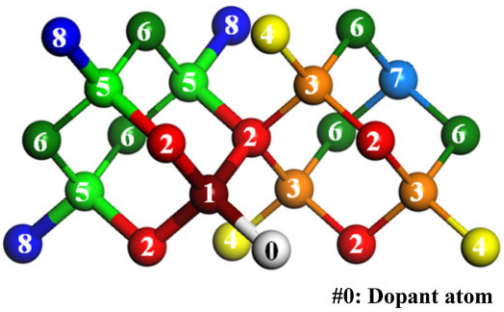

Figure 4 Sites of V from the dopant atom at #0 site in a quarter of 64-atom supercell ($2a \times a \times a$). Zigzag-chains of Si atoms in a $\langle 110 \rangle$ direction include the sites labeled #0, 1, 2, 5, 8 and are shown by thicker bonds.

3.3 Local strain around dopant atoms Figure 5 plots the calculated bond strains along zigzag-chains and bond strains perpendicular to the zigzag-chains (along bonds from the 2nd nearest Si from the dopant) in 216-atom supercells. It is found that (i) C, B, and P atoms with smaller covalent radii than Si form tensile local strain along zigzag-chains, while Ga, Sn, Sb, and Bi atoms with larger covalent radii than Si form compressive local strain. Another important result is that (ii) the local strains of each dopant (except for As) perpendicular to zigzag-chains have opposite signs compared to the strains along zigzag-chains. The local strains for Ge and As dopants are much smaller than those for the other dopants. Furthermore, the absolute values for local strains perpendicular to the zigzag-chains are about 1 order of magnitude smaller than those along zigzag-chains. All the other bonds around each dopant perpendicular to the zigzag-chains show similar tendencies, i.e., far smaller local strains

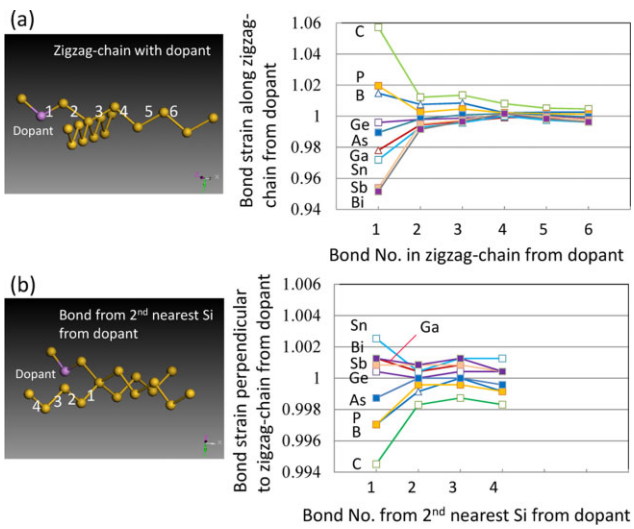

Figure 5 Calculated bond strains (a) along a zigzag-chain from the dopant atom on a Si {110} plane and (b) perpendicular to the zigzag-chain from a dopant atom (along bonds from 2nd nearest Si from dopant) in a 216-atom supercell.

with an opposite sign compared to those along zigzag-chains. When the dopant is smaller than the Si atom, the dopant pulls Si atoms inwards on the 12 zigzag-chains, and compresses the Si–Si bonds between two neighboring zigzag-chains. This means that local strains have a different sign between zigzag-chains and the other bonds. When the dopant atom is larger than a Si atom, the local strain distribution becomes the opposite of that due to the smaller dopant atom.

3.4 Formation energy of intrinsic point defects around a dopant atom Figure 6a–c shows the dependence of the calculated vacancy formation energy on the distance from p-type, neutral, and n-type dopants. The dotted lines from the 1st to the 5th position in these figures indicate the distance from the dopant before the cell size and ionic coordinates are relaxed. It can be confirmed that $E_f^{V,dope}$ at

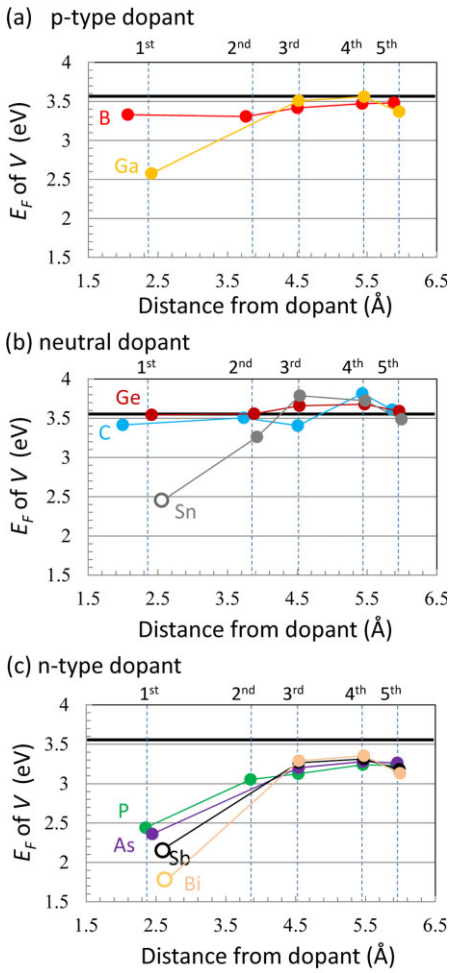

Figure 6 Dependence of calculated vacancy formation energy on the distance from (a) p-type, (b) neutral, and (c) n-type dopant atoms. Horizontal thick full lines indicate the formation energy of Jahn–Teller distortion ($E_f^V = 3.578$ eV) in a perfect Si crystal. Open circles for Sn, Sb, and Bi indicate split vacancies. Dotted lines from 1st to 5th position indicate the distance from the dopant before cell size and ionic coordinates are relaxed.

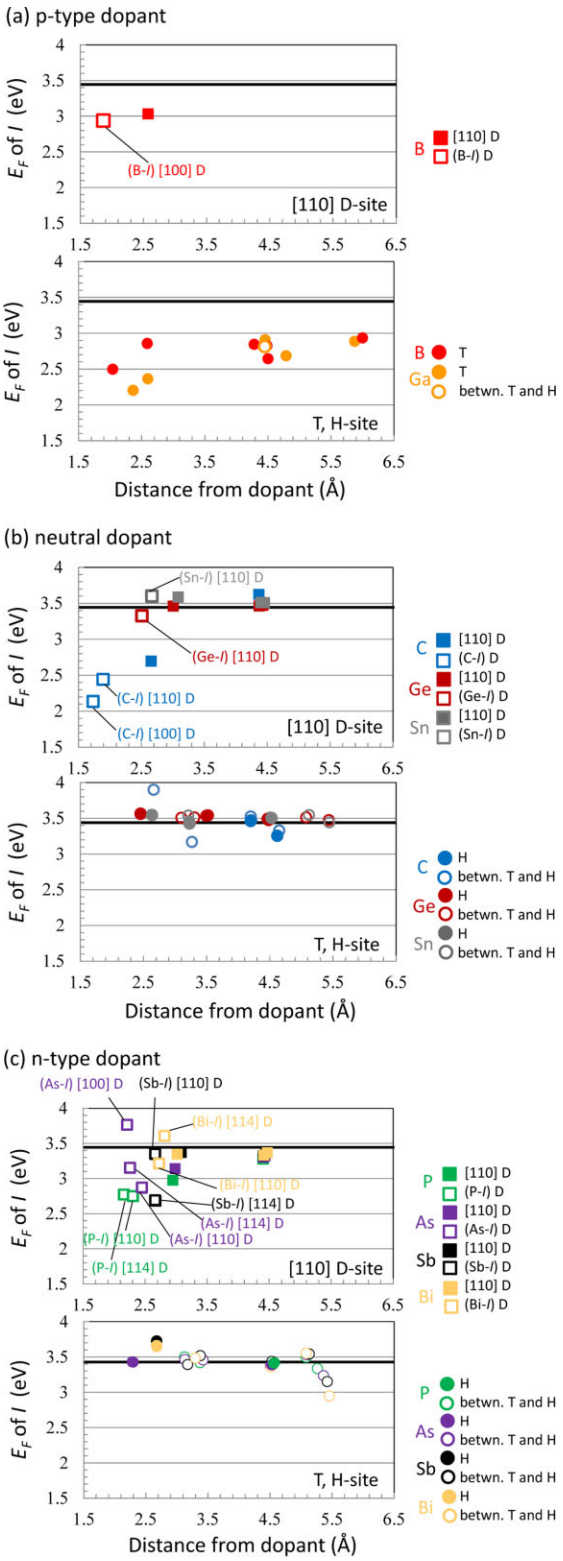

Figure 7 Dependence of calculated self-interstitial formation energy on distance from (a) p-type, (b) neutral, and (c) n-type dopant atoms. Horizontal thick full lines indicate the formation energy of the [110] D-site ($E_f^I = 3.433$ eV) in perfect Si crystal. Closed squares, open squares, closed circles, and open circles correspond to [110] D-site, (dopant-I) D-site, T or H-site, and between T and H-site.

the 1st site differs for the same types of dopants. Note that the formation energy of vacancies with larger dopants is smaller than that with smaller dopants.

Since the electrical state is almost the same for the same types of dopants, this result is mainly due to the difference in local strain. Furthermore, $E_f^{V,dope}$ at and far from the 2nd sites are close for neutral dopants without changing the electrical state, and close to that of V in perfect Si. This indicates that local strain effects effectively are only important at the 1st site from the dopant atom. The type and magnitude of local strain differ for the n-type dopants P, As, Sb, and Bi. However, starting from the 2nd site, $E_f^{V,dope}$ is nearly the same for all n-type dopants and is about 0.3–0.4 eV lower than that in perfect Si. This illustrates that not local strain but the electrical state around n-type dopants mainly determines the V formation energy.

Figure 7a–c shows the dependence of the calculated self-interstitial formation energy on the distance from p-type, neutral, and n-type dopants. $E_f^{I,dope}$ of the [110] D-site around the dopant atom and the D-site of the dopant-I is summarized at the top in the three figures, and $E_f^{I,dope}$ of the T-site, H-site, and between the T- and H-sites is summarized at the bottom.

Stable sites for I are predominantly controlled by the electrical state. That is, self-interstitials for p-type dopants are rather stable at T-sites, while self-interstitials for neutral and n-type dopants are rather stable at D-sites. Furthermore, $E_f^{I,dope}$ differs for the types of dopants as follows.

(1) In case of p-type dopants, $E_f^{I,dope}$ at T-sites up to ~6 Å is reduced by about 0.5–1.3 eV compared to that in perfect Si. No remarkable differences in $E_f^{I,dope}$ are obtained for B and Ga atoms. These results are due to the Coulomb (long-range) interaction between acceptor and positively charged I at T-site.
(2) In case of neutral dopants, $E_f^{I,dope}$ at the D-sites up to ~3 Å from C atom without the electrical state being changed is reduced by about ~0.7 to 1.3 eV compared to that in perfect Si while Ge and Sn atoms have no impact on $E_f^{I,dope}$. These results are due to the larger local (short-range) tensile strain formed by C atoms, which reduce the formation energy of the neutral I at the D-site.
(3) In case of n-type dopants, $E_f^{I,dope}$ at the D-sites up to ~3 Å without the electrical state being changed is reduced by about 0.5 eV compared to that in perfect Si. P, which gives local (short-range) tensile strain, shows the largest impact to the neutral I at D-site among the n-type dopants.

3.5 Dependence of total point defect concentrations on dopant types and concentrations Here, we define the "total V or I" as the sum of free V or I and V or I trapped by the dopants. The thermal equilibrium concentrations of total V and I will change due to the change in the formation energies of point defects around dopant atoms, depending on the concentrations and types of dopants. The total equilibrium V concentration, $C_V^{eq,tot}$,

can be written as:

$$C_{\mathrm{V}}^{\mathrm{eq,tot}} = C_{\mathrm{V,site}}\left[1-\left(1+\sum_{i=1}^{5} Z_i\right)\frac{C_{\mathrm{D}}}{C_{\mathrm{Si}}}\right] \times \exp\left(\frac{S_{\mathrm{f}}^{\mathrm{V,non}}}{k_{\mathrm{B}}}\right)\exp\left(-\frac{E_{\mathrm{f}}^{\mathrm{V,non}}}{k_{\mathrm{B}}T}\right) + C_{\mathrm{D}}\sum_{i=1}^{5} Z_i \exp\left(\frac{S_{\mathrm{f}}^{\mathrm{V}_i,\mathrm{dope}}}{k_{\mathrm{B}}}\right)\exp\left(-\frac{E_{\mathrm{f}}^{\mathrm{V}_i,\mathrm{dope}}}{k_{\mathrm{B}}T}\right) = \exp\left(-\frac{E_{\mathrm{f}}^{\mathrm{V,non}}}{k_{\mathrm{B}}T}\right)\left\{C_{\mathrm{V,site}}\left[1-\left(1+\sum_{i=1}^{5} Z_i\right)\frac{C_{\mathrm{D}}}{C_{\mathrm{Si}}}\right] \times \exp\left(\frac{S_{\mathrm{f}}^{\mathrm{V,non}}}{k_{\mathrm{B}}}\right) + C_{\mathrm{D}}\sum_{i=1}^{5} Z_i \exp\left(\frac{S_{\mathrm{f}}^{\mathrm{V}_i,\mathrm{dope}}}{k_{\mathrm{B}}}\right) \times \exp\left(\frac{E_{\mathrm{f}}^{\mathrm{V,non}} - E_{\mathrm{f}}^{\mathrm{V}_i,\mathrm{dope}}}{k_{\mathrm{B}}T}\right)\right\}. \quad (4a)$$

Here, $C_{\mathrm{V,\ site}} = 5\times10^{22}\,\mathrm{cm}^{-3}$ is the number of possible vacancy sites per unit volume, which equals the number of Si atoms per unit volume, C_{Si}. $S_{\mathrm{f}}^{\mathrm{V,non}}$ and $E_{\mathrm{f}}^{\mathrm{V,non}}$ are the formation entropy and energy of a vacancy for intrinsic Si, respectively. k_{B} is the Boltzmann constant, and T is the temperature. Z_i is the coordination number at the i-th ($i = 1$–5) site, and the sum of $i = 1$–5 is 46 within a sphere with a 6 Å radius around the dopant. C_{D} is the dopant concentration and $S_{\mathrm{f}}^{\mathrm{V}_i,\mathrm{dope}}$ and $E_{\mathrm{f}}^{\mathrm{V}_i,\mathrm{dope}}$ correspond to the formation entropy and energy, respectively, of a vacancy at the i-th site from the dopant. $E_{\mathrm{f}}^{\mathrm{V,non}} - E_{\mathrm{f}}^{\mathrm{V,dope}}$ in the second row of Eq. (4a) is the change in the formation energy of V around the dopant atom compared to the intrinsic value. Unfortunately, no reliable data are available for $S_{\mathrm{f}}^{\mathrm{V}_i,\mathrm{dope}}$. Therefore, it is assumed that $S_{\mathrm{f}}^{\mathrm{V}_i,\mathrm{dope}}$ is equal to $S_{\mathrm{f}}^{\mathrm{V,non}}$ in the analysis that follows.

The formation entropy for self-interstitials I may depend on the site, i.e., the D-, T-, and H-site. We assume that self-interstitials in intrinsic Si occupy [110] D-sites to evaluate their formation entropy. $C_{\mathrm{I}}^{\mathrm{eq,tot}}$ can be approximately written as:

$$C_{\mathrm{I}}^{\mathrm{eq,tot}} \approx C_{\mathrm{I,site}}\left[1-\left(1+\sum_{j=1}^{3} Z_j\right)\frac{C_{\mathrm{D}}}{C_{\mathrm{Si}}}\right] \times \exp\left(\frac{S_{\mathrm{f}}^{\mathrm{I,non}}}{k_{\mathrm{B}}}\right)\exp\left(-\frac{E_{\mathrm{f}}^{\mathrm{I,non}}}{k_{\mathrm{B}}T}\right) + C_{\mathrm{D}}\sum_{j} Z_j^{*} \exp\left(\frac{S_{\mathrm{f}}^{\mathrm{I}_j,\mathrm{dope}}}{k_{\mathrm{B}}}\right)\exp\left(-\frac{E_{\mathrm{f}}^{\mathrm{I}_j,\mathrm{dope}}}{k_{\mathrm{B}}T}\right) = \exp\left(-\frac{E_{\mathrm{f}}^{\mathrm{I,non}}}{k_{\mathrm{B}}T}\right)\left\{C_{\mathrm{I,site}}\left[1-\left(1+\sum_{j=1}^{3} Z_j\right)\frac{C_{\mathrm{D}}}{C_{\mathrm{Si}}}\right] \times \exp\left(\frac{S_{\mathrm{f}}^{\mathrm{I,non}}}{k_{\mathrm{B}}}\right) + C_{\mathrm{D}}\sum_{j} Z_j^{*} \exp\left(\frac{S_{\mathrm{f}}^{\mathrm{I}_j,\mathrm{dope}}}{k_{\mathrm{B}}}\right) \times \exp\left(\frac{E_{\mathrm{f}}^{\mathrm{I,non}} - E_{\mathrm{f}}^{\mathrm{I}_j,\mathrm{dope}}}{k_{\mathrm{B}}T}\right)\right\}. \quad (4b)$$

Here, $C_{\mathrm{I,\ site}} = 3\times10^{23}\,\mathrm{cm}^{-3}$ is the number of the most stable interstitial sites ([110] D-sites) per unit volume. $S_{\mathrm{f}}^{\mathrm{I,non}}$ and $E_{\mathrm{f}}^{\mathrm{I,non}}$ are the formation entropy and energy, respectively, of a self-interstitial at a [110] D-site for intrinsic Si. Z_j is the coordination number at the j-th ($j = 1$–3) site, and the sum of $j = 1$–3 is 28 within the spherical space with a 5 Å radius around the dopant. Z_j is the coordination number of stable interstitial site j depending on the dopant type. $S_{\mathrm{f}}^{\mathrm{I}_j,\mathrm{dope}}$ and $E_{\mathrm{f}}^{\mathrm{I}_j,\mathrm{dope}}$ correspond to the formation entropy and energy, respectively, of a self-interstitial at the interstitial site j. $E_{\mathrm{f}}^{\mathrm{I,non}} - E_{\mathrm{f}}^{\mathrm{I}_j,\mathrm{dope}}$ in the second row of Eq. (4b) is the change in formation energies of I around the dopant atom compared to the intrinsic value. We again assume that $S_{\mathrm{f}}^{\mathrm{I}_j,\mathrm{dope}}$ is equal to $S_{\mathrm{f}}^{\mathrm{I,non}}$ for the same reason as for the vacancy case.

V–I recombination ($\mathrm{V} + \mathrm{I} \rightarrow$ null) leads to an energy gain of 7.012 eV while V_2 formation ($\mathrm{V} + \mathrm{V} \rightarrow \mathrm{V}_2$) leads to an energy gain of 1.725 eV. The estimated temperature range of V–I recombination is higher than 1350 °C [24] while that of V_2 formation is about 1100 °C [5]. The energy gains of the dopant D related reactions, $\mathrm{DI} + \mathrm{V} \rightarrow \mathrm{D}$, $\mathrm{DV} + \mathrm{I} \rightarrow \mathrm{D}$, $\mathrm{D} + \mathrm{I} \rightarrow \mathrm{DI}$, and $\mathrm{D} + \mathrm{V} \rightarrow \mathrm{DV}$ were calculated [11]. Here, DI and DV indicate I and V trapped by the dopant atom, respectively. The first two reactions have energy gains larger than 5.2 eV for the calculated dopants. This indicates that recombination of free V (or I) and dopant-trapped I (or V) occurs at temperatures above the void formation temperature. The last two reactions have energy gains smaller than 1.8 eV. I and V trapped by the dopant atoms will thus easily be released from dopants at temperatures above the void formation temperature. These released V and I will then also recombine at high temperature confirming that the majority of the incorporated intrinsic point defects from the melt recombine in the growing crystal.

3.6 Model of point defect behavior and explanation of experimental results The discussion below leads to an appropriate model to predict point defect behavior in a heavily doped Si single crystal growing from a melt. The incorporated total V and I concentrations at melting point depend on the type and concentration of the dopant. Most of the introduced V and I will recombine at temperatures above the formation temperature of voids (~1100 °C) or I-clusters (~1000 °C).

The Voronkov model suggests that $C_{\mathrm{V}}^{\mathrm{eq,tot}}(T_{\mathrm{m}}) - C_{\mathrm{I}}^{\mathrm{eq,tot}}(T_{\mathrm{m}})$ determines the dominant type of intrinsic point defects in the growing crystal. Figure 8 plots the calculated dependence of $C_{\mathrm{V}}^{\mathrm{eq,tot}}(T_{\mathrm{m}}) - C_{\mathrm{I}}^{\mathrm{eq,tot}}(T_{\mathrm{m}})$ on dopant type and concentration using the present model.

It has been reported [4, 5] that the OSF ring radius in p-type CZ-Si shrinks when the B concentration is higher than $\sim1\times10^{18}\,\mathrm{B\,cm}^{-3}$ and that the crystals becomes I-rich (the OSF ring disappearing in the crystal center) for B concentrations higher than $\sim1\times10^{19}\,\mathrm{B\,cm}^{-3}$. The results in the present paper reveal that the value of $C_{\mathrm{V}}^{\mathrm{eq,tot}}(T_{\mathrm{m}}) - C_{\mathrm{I}}^{\mathrm{eq,tot}}(T_{\mathrm{m}})$ starts to decrease at $\sim1\times10^{18}\,\mathrm{B\,cm}^{-3}$ and becomes negative at $\sim2\times10^{19}\,\mathrm{B\,cm}^{-3}$ in excellent quantitative agreement with the experiment. In near intrinsic Si,

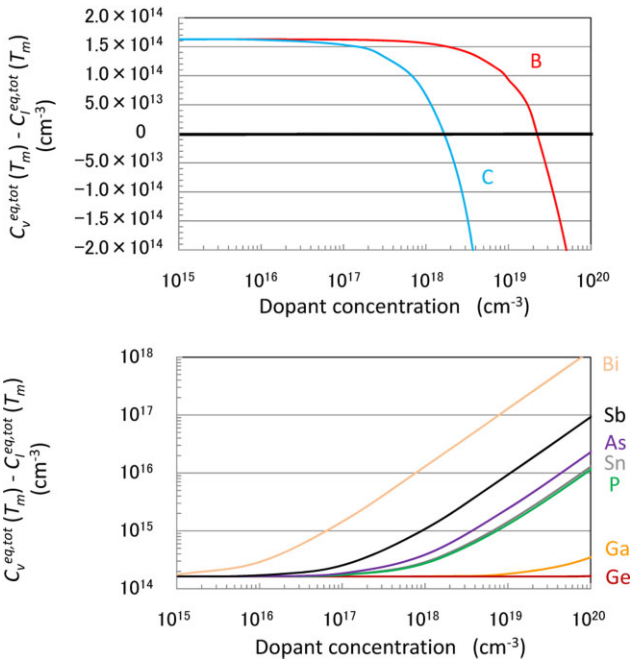

Figure 8 Calculated dependence at melting temperature of Si of $C_V^{eq,tot}(T_m) - C_I^{eq,tot}(T_m)$ on dopant concentration and type. Intrinsic point defect parameters proposed by Nakamura et al. [14] are used.

Nakamura et al. [5] found that the V-rich region in CZ-Si becomes narrower for $6 \times 10^{16}\,cm^{-3}$ C doping. Abe [19] made a similar observation in FZ-Si for $5 \times 10^{16}\,C\,cm^{-3}$. Vanhellemont et al. [20] reported that Ge doping at $1 \times 10^{20}\,Ge\,cm^{-3}$ in CZ-Si has only a small impact on the V concentration. The calculated results shown in Fig. 8 also quantitatively explain these experimental results. For n-type Si, Sugimura et al. [25] reported that the void density and size increased in CZ-Si due to doping with As concentrations above $\sim 2 \times 10^{18}\,As\,cm^{-3}$. Similar results were obtained by Nakamura et al. [5] for As and P doping. Abe [19] demonstrated that the D-defect region in FZ-Si became wider due to Sb concentrations higher than $1 \times 10^{17}\,cm^{-3}$ while doping with $10^{15}\,cm^{-3}$ Bi had no impact. Furthermore, Abe [19] found that the effect of $1 \times 10^{18}\,cm^{-3}$ Sb doping on D-defects was similar as that of doping with $3 \times 10^{18}\,cm^{-3}$ Sn. The calculated results shown in Fig. 8 also quantitatively explain these experimental results for n-type (and Sn) doping.

In the Voronkov criterion given in Eq. (1), we assume in case of heavy doping that (i) $C_i(T_m) = C_i^{eq}(T_m) = C_i^{eq,tot}(T_m)$ (i = I or V), (ii) E_f^I and E_f^V are the intrinsic values for the formation energy of I and V, respectively, and (iii) D_I and D_V are not affected by dopant atoms.

Figure 9 plots the dependence on dopant concentration of $(v/G)_{crit}$ normalized with respect to the intrinsic value $(v/G)^0_{crit}$. The circles in the figures for B and C doping are the experimental results obtained by Nakamura et al. [5]. The calculated results for heavy B doping agree well with the experimental results. Although there is only one experimental plot for C doping, it is also close to the calculated line. To the best of our knowledge, no experimental results for the impact of n-type dopants on critical $(v/G)_{crit}$ have yet been reported in literature.

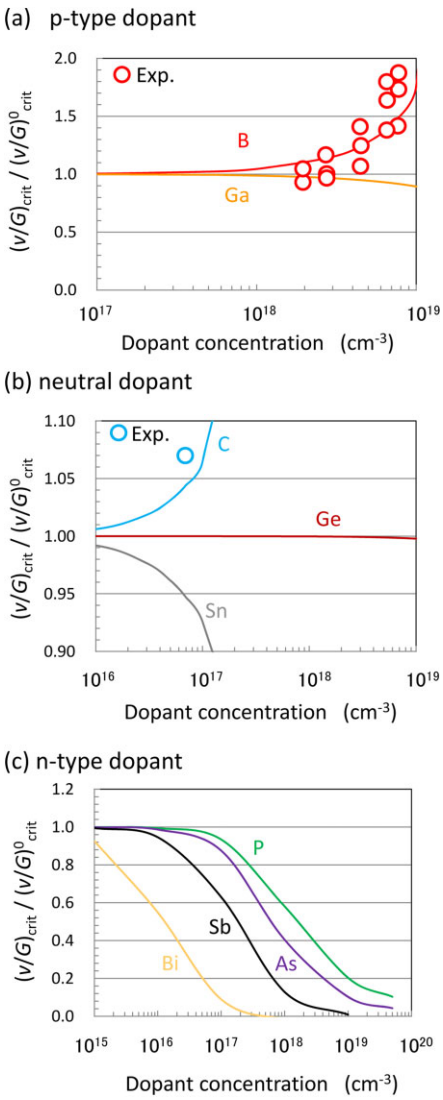

Figure 9 Calculated dependence of critical $(v/G)_{crit}$ on dopant concentration normalized with respect to the intrinsic value using the parameters proposed by Nakamura et al. [14]. Results are shown for the most common p-type dopants (a), neutral dopants (b) and n-type dopants (c). Open circles for B and C doping in (a) and (b), respectively, are published experimental data.

Summarizing the main results: using results from DFT calculations, a model was proposed explaining quantitatively the intrinsic point defect behavior in heavily doped Si single crystals growing from a melt:

(1) The incorporated total V and I (sum of free V or I and V or I around the dopants) concentrations at melting temperature depend on the type and concentration of dopant. This is due to the change in the formation

energies of V and I around the dopant atoms, which is caused by the electrical state and magnitude of local strain depending on the types and sizes of the dopant.

(2) Most of the total V and I concentrations contribute to pair recombination at much higher temperatures than those at which voids are formed (1100 °C). This means that the values of $C_V^{eq,tot}(T_m)$ and $C_I^{eq,tot}(T_m)$ determine the impact of the dopant type and concentration on the dominant point defect and also the critical $(v/G)_{crit}$.

The main strength of the proposed model is that it explains point defect behavior for all dopants and for all concentrations.

4 Remaining problems In this section, we discuss the main remaining problems related to the topics of this paper.

4.1 Unified model for the impact of thermal stress and doping In order to explain and engineer the intrinsic point defect behavior in large-diameter single crystal Si growing from a melt, a unified model valid for all pulling processes, crystal resistivities and not electrically active impurity concentrations is needed by coupling the impacts of thermal stress and dopant atoms [26]. These two impacts cannot be simply superimposed due to the complicated local strain and electronic state around dopant atoms. Furthermore one should also take into account the impact of the different charge states of the intrinsic point defects, in particular during the initial cooling of the crystal.

4.2 Determination of intrinsic point defect parameters for zero stress The intrinsic point defect parameters where extracted from single crystal growth experiments which obviously never occur in stress-free conditions and thus implicitly already contain partly the effect of stress. Further theoretical and experimental studies are needed [27].

4.3 Clarification of the mechanism of impact of interstitial oxygen and nitrogen atoms The mechanism of the increase of $(v/G)_{crit}$ by interstitial oxygen and nitrogen atoms [5] should be clarified as the CZ-Si crystals always contain interstitial oxygen and in most cases contain interstitial nitrogen atoms. A similar approach as used for substitutional dopants in the present work will be useful to clarify the fundamental mechanisms.

4.4 Establishment of a prediction method for the process window for defect-free Si growth It is very useful to be able to predict the process windows for defect-free Si growth for all kind of Si wafer specifications. The impact of electrically active dopants, interstitial oxygen, and nitrogen on grown-in defect formation, for example, (i) B atoms extend the I-rich defect-free regions, and (ii) N atoms extend both V-rich and I-rich defect-free regions [5], should be clarified and quantified.

5 Conclusions In this paper, we have reviewed our recent studies of the dependence of Voronkov criterion on thermal stress and doping by using DFT based calculations. The calculated plane stress dependence is in excellent agreement with the published experimental values and should be taken into account in the development of pulling processes for 450 mm diameter defect-free Si crystals. It was shown that it is in principle also possible to predict the process window for defect-free Si crystal growth.

The mechanisms behind the experimentally observed impact of the type and concentration of substitutional dopants on intrinsic point defect behavior and formation of grown-in defects are clarified. On the basis of intrinsic point defect properties calculated by DFT, a generally valid model of intrinsic point defect behavior in a pulled heavily doped Si crystal is proposed. Main conclusions are that (i) the incorporated total V and I concentrations at the melting point depend on the types and concentrations of dopants and (ii) most of the total V and I concentrations contribute to Frenkel pair recombination during Si crystal growth at temperatures much higher than those to form grown-in intrinsic point defect clusters. The Voronkov model, while taking into account the present improvements, clearly explains all reported experimental results on grown-in defects for heavily doped Si crystal growth from a melt.

Finally, we have also discussed the main remaining problems that have to be solved in order to improve crystal growth simulation capabilities that are essential for the future development ultra large diameter Si crystals.

Acknowledgements The authors wish to thank Dr. Katsuto Tanahashi (Fujitsu Semiconductor Limited) for invaluable discussions and Mr. Ryo Matsutani for figure preparation. This work was partially supported by JSPS KAKENHI Grant Number 25390069.

References

[1] V. V. Voronkov, J. Cryst. Growth **59**, 625 (1982).
[2] V. V. Voronkov and R. Falster, J. Appl. Phys. **86**, 5975 (1999).
[3] K. Nakamura, R. Suewaka, and B. Ko, ECS Solid State Lett. **3**, N5 (2014).
[4] E. Dornberger, D. Graef, M. Suhren, U. Lambert, P. Wagner, F. Dupret, and W. von Ammon, J. Cryst. Growth **180**, 343 (1997).
[5] K. Nakamura, R. Suewaka, T. Saishoji, and J. Tomioka, in: Proc. Forum on the Science and Technology of Silicon Materials 2003, edited by H. Yamada-Kaneta and K. Sumino (Japan Technical and Information Service, 2003), p. 161 and references therein.
[6] J. Vanhellemont, J. Appl. Phys. **110**, 063519 (2011); J. Appl. Phys. **110**, 129903 (2011); J. Appl. Phys. **111**, 116103 (2012).
[7] E. Kamiyama, K. Sueoka, and J. Vanhellemont, J. Appl. Phys. **111**, 083507 (2012); E. Kamiyama, K. Sueoka, J. Vanhellemont, Phys. Status Solidi A **209**, 1880 (2012).
[8] K. Sueoka, E. Kamiyama, and H. Kariyazaki, J. Appl. Phys. **111**, 093529 (2012).

[9] K. Sueoka, E. Kamiyama, and J. Vanhellemont, J. Cryst. Growth **363**, 97 (2013).
[10] K. Sueoka, E. Kamiyama, J. Vanhellemont, and K. Nakamura, ECS Solid State Lett. **3**, 69 (2014).
[11] K. Sueoka, E. Kamiyama, and J. Vanhellemont, J. Appl. Phys. **114**, 153510 (2013) and references therein.
[12] K. Nakamura, unpublished results.
[13] G. Watkins, Mater. Res. Soc. Symp. Proc. **469**, 139 (1997).
[14] K. Nakamura, T. Saishoji, and J. Tomioka, ECS Proc. PV **2002-2**, 554 (2002).
[15] M. Hourai, E. Kajita, T. Nagashima, H. Fujiwara, S. Ueno, S. Sadamitsu, S. Miki, and T. Shigematsu, Mater. Sci. Forum **196–201**, 1713 (1995).
[16] M. Hourai, H. Nishikawa, T. Tanaka, S. Umeno, E. Asayama, T. Nomachi, and G. Kelly, in: Semiconductor Silicon 1998, PV 98-1, edited by H. R. Huff (The Electrochem. Soc. Proc. Ser., Pennington, NJ, 1998), p. 453.
[17] A. J. R. de Kock, W. T. Stacy, and W. M. van de Wijgert, Appl. Phys. Lett. **34**, 611 (1979).
[18] T. Abe, H. Harada, and J. Chikawa, Mater. Res. Soc. Proc. **14**, 1 (1983).
[19] T. Abe, J. Cryst. Growth **334**, 4 (2011).
[20] J. Vanhellemont, X. Zhang, W. Xu, J. Chen, X. Ma, and D. Yang, J. Appl. Phys. **108**, 123501 (2010).
[21] K. Tanahashi, N. Inoue, and Y. Mizokawa, Physica B **308–310**, 502 (2001).
[22] K. Tanahashi, H. Harada, A. Koukitsu, and N. Inoue, J. Cryst. Growth **225**, 294 (2001).
[23] J. Vanhellemont, E. Kamiyama, and K. Sueoka, ECS J. Solid State Sci. Technol. **2**, 166 (2013) and references therein.
[24] T. Saishoji, K. Nakamura, H. Nakajima, T. Yokoyama, F. Ishikawa, and J. Tomioka, in: High Purity Silicon V, PV 98-13 (The Electrochem. Soc. Proc. Ser., Pennington, NJ, 1998), p. 28.
[25] W. Sugimura, T. Ono, S. Umeno, M. Hourai, and K. Sueoka, ECS Trans. **2**, 95 (2006).
[26] J. Vanhellemont, E. Kamiyama, and K. Sueoka, ECS J. Solid State Sci. Technol. **2**, 166 (2013).
[27] J. Vanhellemont, E. Kamiyama, and K. Sueoka, ECS Solid State Lett. **3**, X3 (2014).

